New Insights into FAK Signaling and Localization Based on Detection of a FAT Domain Folding Intermediate

Richard D.S. Dixon,[1,7] Yiwen Chen,[2,7] Feng Ding,[1]
Sagar D. Khare,[1] Kirk C. Prutzman,[1]
Michael D. Schaller,[3,4,5,6] Sharon L. Campbell,[1,4,*]
and Nikolay V. Dokholyan[1,*]
[1]Department of Biochemistry and Biophysics
[2]Department of Physics and Astronomy
[3]Department of Cell and Developmental Biology
[4]Lineberger Comprehensive Cancer Center
[5]Comprehensive Center for Inflammatory Disorders
[6]Carolina Cardiovascular Biology Center
University of North Carolina at Chapel Hill
Chapel Hill, North Carolina 27599

Summary

Mounting evidence suggests that the focal adhesion targeting (FAT) domain, an antiparallel four-helix bundle, exists in alternative conformations that may modulate phosphorylation, ligand binding, and the subcellular localization of focal adhesion kinase (FAK). In order to characterize the conformational dynamics of the FAT domain, we have developed a novel method for reconstructing the folding pathway of the FAT domain by using discrete molecular dynamics (DMD) simulations, with free energy constraints derived from NMR hydrogen exchange data. The DMD simulations detect a folding intermediate, in which a cooperative unfolding event causes helix 1 to lose helical character while separating from the helix bundle. The conformational dynamic features of helix 1 in the intermediate state of the FAT domain are likely to facilitate Y926 phosphorylation, yet interfere with paxillin binding. The presence of this intermediate state in vivo may promote FAK signaling via the ERK/MAPK pathway and by release of FAK from focal adhesions.

Introduction

Focal adhesion kinase (FAK) is a nonreceptor tyrosine kinase that is expressed in most tissues and is regulated by integrin-dependent cell adhesion (Parsons, 2003). FAK functions in the control of several important biological processes, e.g., cell migration and apoptosis (Schaller, 2001), and FAK is overexpressed in many forms of cancer (Gabarra-Niecko et al., 2003). The correct localization of FAK to focal adhesions is required for integrin-dependent regulation of FAK and for FAK to direct tyrosine phosphorylation of downstream substrates (Cooley et al., 2000; Shen and Schaller, 1999). The C terminus of FAK contains a focal adhesion targeting (FAT) domain, which is a four-helix bundle structural motif (Hayashi et al., 2002; Liu et al., 2002; Prutzman et al., 2004), that is responsible for subcellular localization of FAK (Hildebrand et al., 1993).

*Correspondence: campbesl@med.unc.edu (S.L.C.); dokh@med. unc.edu (N.V.D.)
[7]These authors contributed equally to this work.

The avian FAT domain contains a tyrosine in helix 1 at position 926 (925 in the human and mouse sequences) that is a substrate for phosphorylation by Src. Phosphorylation of Y926 creates a docking site for the SH2 domain of Grb2 (Schlaepfer and Hunter, 1996), and the FAT/Grb2 interaction is one of the mechanisms linking FAK to the Ras/MAPK signaling pathway (Schlaepfer and Hunter, 1997). Structural studies indicate that Src-like tyrosine kinases bind to substrates in a β strand conformation (Brown et al., 1999; Hubbard, 1997). Further structural studies demonstrated that tyrosine-phosphorylated ligands form a β turn to facilitate binding interactions with the Grb2 SH2 domain (Kuriyan and Cowburn, 1997). Results from these studies suggest that the region around Y926 must adopt an extended conformation for phosphorylation and association with Grb2. There has been speculation (Arold et al., 2002; Liu et al., 2002; Prutzman et al., 2004) that for phosphorylation of Y926 and subsequent Grb2 binding to occur, the FAT domain must pass through an "open" conformation in which helix 1 extends from the four-helix bundle, allowing the region flanking tyrosine 926 to adopt the necessary conformation.

While X-ray crystal (Arold et al., 2002; Hayashi et al., 2002) and NMR structures (Liu et al., 2002; Prutzman et al., 2004) reveal a four-helix bundle fold for the FAT domain, a second structure has also been described. One of the reported crystal structures (Arold et al., 2002) is a dimer that has undergone "domain exchange," in which the N terminus and helix 1 of one molecule associate with helices 2–4 of the other symmetry-related molecule. The formation of the domain-exchanged dimer was speculated to proceed through an intermediate state in which helix 1 transiently separates from the core bundle (Arold et al., 2002). The intermediate state of the FAT domain that promotes formation of the domain-swapped dimer may also facilitate phosphorylation at tyrosine 926 and Grb2 binding (Arold et al., 2002). NMR studies of the FAT domain in solution revealed that residues at the carboxy terminus of helix 1, loop 1, and the amino terminus of helix 2 (residues 941–951) showed line broadening that was consistent with conformational exchange on the NMR timescale (Prutzman et al., 2004). The loop region between helices 1 and 2 was consequently identified as a putative "hinge region" that may be responsible for promoting a partially unfolded intermediate state, similar to the intermediate state that would produce the domain-swapped dimer. However, detection and characterization of such protein intermediate states is often nontrivial.

Although weakly populated protein-folding intermediates are often difficult to structurally characterize, hydrogen exchange methods have proven to be a powerful technique for identifying and characterizing kinetic and equilibrium folding intermediates (Bai et al., 1995; Chamberlain et al., 1996), but these methods are limited in their ability to describe the structure of the intermediates. By combining hydrogen exchange data with DMD simulations, we have been able to capture structural details of

the intermediate state ensemble for FAT domain folding, which has allowed us to reconstruct the conformers that we believe are important for FAK signaling through the FAT domain.

Hydrogen Exchange Measurements

The relationships between the hydrogen exchange rates, transient unfolding mechanisms, and the structural stability of proteins have been previously described (Bai et al., 1994; Maity et al., 2003). The exchange rates of backbone amide protons are commonly expressed as protection factors, $P_f = k_{rc}/k_{ex}$, where k_{ex} is the experimentally measured hydrogen exchange rate and k_{rc} is the intrinsic rate of hydrogen exchange in the unstructured protein. Protection factors can be calculated by using the method presented by Bai and coworkers (Bai et al., 1993). In the EX2 limit, usually satisfied when the structure of the protein is stable, the protection factor is equivalent to the equilibrium constant for the unfolding transition that makes the amide hydrogen exchange competent. In this case, the protection factors may be used to calculate the free energy of the structural opening event:

$$\Delta G_{HX} = -RT \ln P_f. \tag{1}$$

Here, protection factors derived from hydrogen exchange data were used as experimental constraints in discrete molecular dynamics simulations of the FAT domain-folding process.

Simulating Protein Folding Using the Gō Model

An atomic resolution simulation of the protein-folding process by using traditional molecular mechanics forcefields is difficult by direct computational approaches because of the vast dimensionality of the protein conformational space (Karplus and Shakhnovich, 1994). Simplified models, such as the Gō model (Abe and Gō, 1981; Gō and Abe, 1981), provide a powerful alternative to study protein folding because of their ability to simulate folding on computationally tractable timescales and to reproduce both folding thermodynamics and kinetics in agreement with experiments (Borreguero et al., 2002; Ding et al., 2002a). In the Gō model (see the Experimental Procedures), the energy of the protein is expressed as a sum of pairwise contact energies so that the ground state corresponds to the native state of the protein. In the *unscaled* Gō model, the strengths of interactions among native contacts are equal. Such a simplified scheme of assigning strengths of interactions may lead to discrepancy between simulation and experiment in protein-folding dynamics, due to the heterogeneity in contact energies (Khare et al., 2003). Several schemes have been developed to assign the strengths of interactions in order to take the contact energy heterogeneity into account (Clementi et al., 2003; Karanicolas and Brooks, 2002; Khare et al., 2003). Here, a novel method is presented that uses experimental hydrogen exchange data to scale the interaction energies in the Gō model. The *scaled G*ō model was used to reconstruct and characterize the intermediate state ensemble associated with FAT domain folding, which we postulate to be functionally relevant given the correlation with recent data on FAT conformational dynamics and conformation

plasticity believed to modulate FAT ligand binding, localization, and phosphorylation (Arold et al., 2002; Liu et al., 2002; Prutzman et al., 2004).

Incorporating Protection Factors into the Gō Model

A thorough derivation of this method is described in the Experimental Procedures. In brief, the protection factors obtained from hydrogen exchange experiments can provide the free energy associated with the stability of the protein at each amino acid residue, provided that the amide protons are in the EX2 limit (Bai et al., 1994). In the Gō model, an attractive potential is assigned to each native contact, the sum of which gives the total energy of the protein. The free energy difference between the folded and unfolded states of the protein can be determined at each amino acid from the sum of the potentials of the native contacts in which the amino acid residue participates. A cost function was used to describe the difference in the free energy values derived from the protection factors and the free energy values calculated by taking the summation over the potentials of the native contacts. A Monte Carlo minimization of the cost function was then used to obtain the set of potentials that is most consistent with the experimental protection factors.

Results

Hydrogen Exchange Protection Factors

The FAT domain construct used in these experiments contains 146 residues, including a 12 residue linker at the N terminus (Prutzman et al., 2004). By subtracting the number of prolines from the total number of residues in the expressed FAT domain construct, 138 amide protons are potentially detectable. We were unable to unambiguously assign 20 of the residues in the ^1H-^{15}N HSQC spectrum. Therefore, 118 residues were potential reporter sites for the local stability of the protein structure using hydrogen exchange. The ^1H-^{15}N HSQC spectrum of the FAT domain, illustrated in Figure 1A, shows the observable NH resonances associated with the backbone amides and side chain amines. At the first time point in the real-time hydrogen exchange experiment (Figure 1B), 48 residues were assigned, and for each of these residues, a protection factor was determined. From the remaining 70 residues, 18 residues had hydrogen exchange rates that were fast enough to be observed by using the CLEANEX-PM (Hwang et al., 1997, 1998) experiment with HSQC detection (Figure 1C). The remaining 52 residues had hydrogen exchange rates that were too slow ($k_{ex} \leq 6$ min^{-1}) to be observed by using the CLEANEX-PM experiment and too fast ($k_{ex} \geq 0.1$ min^{-1}) to be measured in real-time by using our methods. A summary of the hydrogen exchange rates determined by the real-time hydrogen exchange experiment and the resulting protection factors used in the DMD simulations is presented in Table 1 (see the Supplementalal Data available with this article online for a complete list).

In Figure 2, a C^α trace of the native-folded FAT domain, which has been color-coded according to the natural logarithm of the experimental protection factors, is
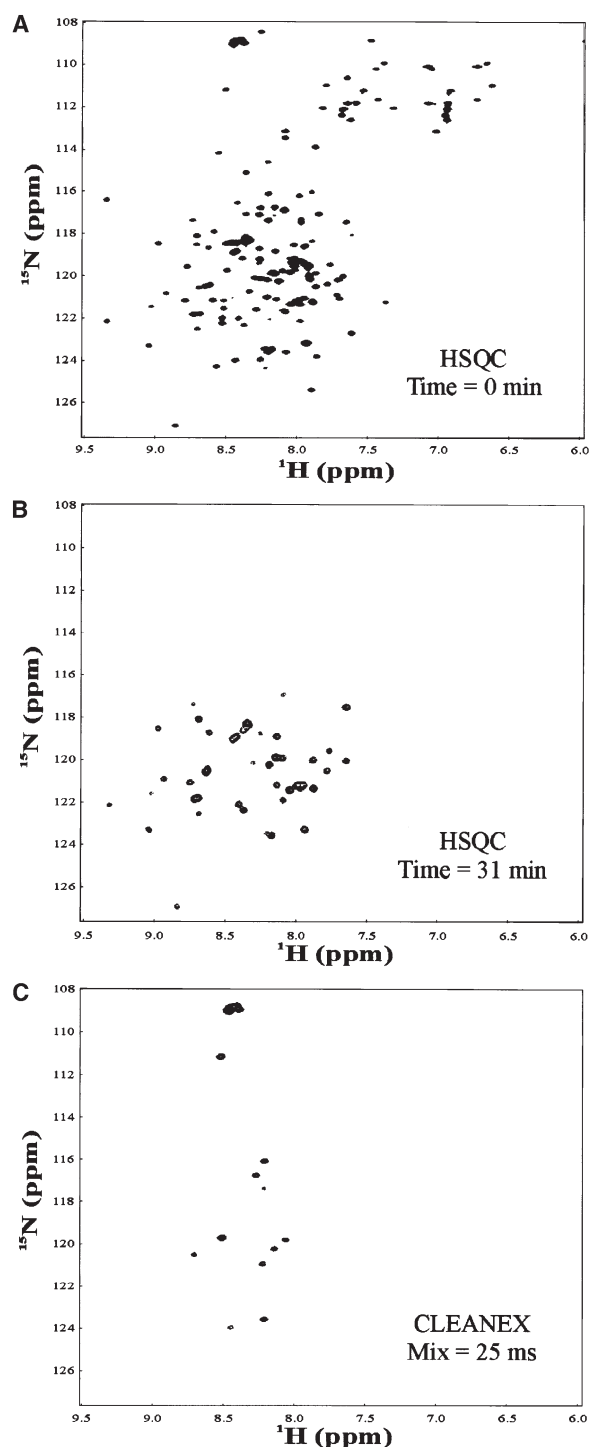
Figure 1. HX NMR Spectra

2D ^{1}H-^{15}N NMR spectra of the avian FAT domain used to calculate hydrogen exchange rates of the backbone amide protons.

(A) HSQC in 90% H_2O/10% D_2O (before exchange to a deuterated solvent) shows the resonance signals for all ^{1}H nuclei attached to ^{15}N nuclei.

(B) HSQC in 95% D_2O/5% H_2O after 31 min (first time point) shows the resonance signals that can be monitored for loss of signal in real time.

(C) CLEANEX-PM with HSQC detection in 90% H_2O/10% D_2O identifies amide protons that exchange rapidly enough to be observed by using polarization transfer.

shown. The regions in yellow are the residues whose amide proton can be observed by using the CLEANEX-PM experiment; in these regions, protein structure has little or no effect on the rate of hydrogen exchange. The regions in red correspond to the residues that have amide protons for which protection factors were not determined because the rate of hydrogen exchange is too slow for the CLEANEX-PM experiment and too fast for the real-time experiments. The blue regions correspond to residues associated with amide resonances for which protection factors were determined from the hydrogen exchange rates measured in real-time, with a color gradient indicating the degree of protection. Proline residues and residues containing amide protons that were not assigned were colored black. These results indicate that the most solvent-protected backbone resonances (blue) are located exclusively in the helical regions of the FAT domain, whereas the least-protected regions (yellow) correspond to amide protons in which amide hydrogen exchange is not significantly slowed by the structure of the protein and are concentrated at the terminal ends of the FAT domain.

In the EX2 limit, the most-protected amide protons exchange through a transient global unfolding of the protein and can, therefore, be used to determine the global stability of the protein. In the case of the FAT domain, the most-protected residue (M1046) has a free energy of hydrogen exchange corresponding to 7.08 $\pm$ 0.03 kcal/mol (Table 1). The uncertainty we report is based solely on the measurement of k_{ex}, while estimates of the error in ΔG_{HX} associated with the uncertainty in k_{rc} values range from about 0.4 kcal/mol (Mayne and Englander, 2000) to less than 0.1 kcal/mol (Milne et al., 1998). The free energy of unfolding was also assessed by monitoring the loss of helical content as a function of increasing guanidine hydrochloride (GdnHCl) concentration by using CD spectroscopy. Data derived from chemical denaturation of the FAT domain were fit by using the linear extrapolation method with global fitting (Santoro and Bolen, 1988) (see the Supplemental Data), and a free energy of unfolding corresponding to a value of 6.3 $\pm$ 0.5 kcal/mol was obtained. The presence of partially unfolded intermediates may lead to a discrepancy between the global stability of the protein determined from HX and by classical unfolding experiments (Mayne and Englander, 2000).

Scaled Gō Model
A native contact is made if the C^β (or C^α in the case of glycine) atoms of two residues are within 7.5 Å of each other in the native, folded state Figure 3. For each native contact, a contact potential was assigned. The native contacts that were strengthened in the scaled Gō model are shown in the lower right triangle of Figure 4A. After generating a set of scaled contact potentials $\{\epsilon_{ij}\}$ (as described in the Experimental Procedures), we verified that our set was consistent with the experimental protection factors. Therefore, the contact frequencies, f_{ij}^F, from the trajectories at low simulation temperature, where the folded state is highly populated, were combined with the potentials $\{\epsilon_{ij}\}$ set according to Equation 3 to produce calculated protection factors. The calculated protection factors show a strong correlation to the ex-

Table 1. Hydrogen Exchange Data Taken from Real-Time NMR Experiments

Residue	k_{ex} (10^3 min^{-1})	k_{rc} (min^{-1})	P_f	$\ln(P_f)$	ΔG_{HX}
Helix 1					
L932	64 ± 5	18.4	290 ± 20	5.7 ± 0.1	3.51 ± 0.06
K934	12.4 ± 0.9	31.3	2,500 ± 100	7.82 ± 0.04	4.82 ± 0.02
A935	15 ± 1	62.4	4,200 ± 300	8.34 ± 0.07	5.14 ± 0.04
V936	8 ± 3	9.44	1,000 ± 500	6.9 ± 0.5	4.3 ± 0.3
I937	4 ± 3	6.38	2,000 ± 3,000	7.6 ± 0.9	4.7 ± 0.6
Helix 2					
G959	14 ± 1	63.8	4,600 ± 300	8.44 ± 0.07	5.20 ± 0.04
L960	13 ± 2	18.4	1,400 ± 200	7.2 ± 0.1	4.43 ± 0.06
A961	20 ± 4	29.2	1,500 ± 300	7.3 ± 0.2	4.5 ± 0.1
L962	2.7 ± 0.4	12.4	4,600 ± 700	8.4 ± 0.2	5.2 ± 0.1
L965	22 ± 3	19.7	900 ± 100	6.8 ± 0.1	4.19 ± 0.06
L966	12 ± 1	7.67	640 ± 50	6.46 ± 0.08	3.98 ± 0.05
A967	4.9 ± 0.4	29.2	6,000 ± 500	8.70 ± 0.08	5.36 ± 0.05
T968	80 ± 30	40.3	500 ± 200	6.2 ± 0.4	3.8 ± 0.2
D970	50 ± 20	18.2	400 ± 200	6.0 ± 0.5	3.7 ± 0.3
L973	30 ± 10	24.8	800 ± 300	6.7 ± 0.4	4.1 ± 0.2
Helix 3					
E985	9.4 ± 0.8	9.71	1,000 ± 90	6.91 ± 0.09	4.26 ± 0.05
A987	4.7 ± 0.3	60.9	13,000 ± 800	9.47 ± 0.06	5.83 ± 0.04
Q988	2.05 ± 0.08	54.3	27,000 ± 1,000	10.20 ± 0.04	6.28 ± 0.02
L990	7.9 ± 0.6	16.4	2,100 ± 200	7.6 ± 0.1	4.68 ± 0.06
S993	49	232	4,700	8.46	5.2
D994	8.0 ± 0.8	50.2	6,300 ± 600	8.7 ± 0.1	5.36 ± 0.06
L995	1.71 ± 0.06	8.62	5,000 ± 200	8.52 ± 0.04	5.25 ± 0.02
A996	2.6 ± 0.2	29.2	11,000 ± 900	9.31 ± 0.08	5.73 ± 0.05
E997	1.57 ± 0.06	16.5	10,500 ± 400	9.26 ± 0.04	5.70 ± 0.02
L998	0.15 ± 0.03	9.61	60,000 ± 10,000	11.0 ± 0.2	6.8 ± 0.1
I999	0.23 ± 0.03	5.43	24,000 ± 3,000	10.1 ± 0.1	6.22 ± 0.06
N1000	4.1 ± 0.1	86.1	21,000 ± 500	9.95 ± 0.02	6.13 ± 0.01
K1001	13 ± 3	90.1	7,000 ± 2,000	8.9 ± 0.3	5.5 ± 0.2
M1002	3.6 ± 0.3	60.9	17,000 ± 1,000	9.74 ± 0.06	6.00 ± 0.04
K1003	23 ± 7	55.6	2,400 ± 800	7.8 ± 0.3	4.8 ± 0.2
L1004	22 ± 3	16.4	700 ± 100	6.6 ± 0.1	4.07 ± 0.06
A1005	41	29.2	710	6.6	4.1
Q1007	19 ± 2	86.1	4,500 ± 500	8.4 ± 0.1	5.17 ± 0.06
Helix 4					
Q1015	53	86.1	1,600	7.4	4.6
Q1020	13 ± 6	71.6	6,000 ± 3,000	8.6 ± 0.7	5.3 ± 0.4
M1021	97	73.3	760	6.6	4.1
L1022	11 ± 1	16.0	1,500 ± 100	7.3 ± 0.4	4.50 ± 0.04
H1026	15 ± 6	37.6	3,000 ± 1000	8.0 ± 0.3	4.9 ± 0.2
L1028	1.01 ± 0.04	12.4	12,300 ± 500	9.42 ± 0.04	5.80 ± 0.02
A1029	0.95 ± 0.05	29.2	31,000 ± 2,000	10.34 ± 0.06	6.37 ± 0.04
D1031	0.83 ± 0.07	18.2	22,000 ± 2,000	10.00 ± 0.09	6.16 ± 0.06
A1032	3.3 ± 0.6	32.8	10,000 ± 2,000	9.2 ± 0.2	5.7 ± 0.1
K1033	1.22 ± 0.06	43.1	35,000 ± 2,000	10.47 ± 0.06	6.45 ± 0.04
L1036	0.20 ± 0.03	18.4	90,000 ± 10,000	11.4 ± 0.1	7.02 ± 0.06
D1037	14 ± 4	15.5	1,100 ± 300	7.0 ± 0.3	4.3 ± 0.2
V1038	1.10 ± 0.05	6.54	5,900 ± 300	8.68 ± 0.05	5.35 ± 0.03
I1039	0.46 ± 0.03	6.38	14,000 ± 900	9.55 ± 0.06	5.88 ± 0.04
D1040	10 ± 1	14.8	1,500 ± 100	7.31 ± 0.07	4.50 ± 0.04
M1046	0.62 ± 0.06	60.9	100,000 ± 10,000	11.5 ± 0.1	7.08 ± 0.06

The residues listed are located exclusively within the helical regions of the FAT domain and were used to scale the pairwise contact energies in the DMD simulations. The experimental rates (k_{ex}) were determined from the decrease in NMR peak intensities in fHSQC spectra over a period of 45.5 hr. The random coil hydrogen exchange rates (k_{rc}) were calculated by using the method of Bai and coworkers (Bai et al., 1993). The errors propagated in Table 1 are based solely on the uncertainty in the experimental measurement of k_{ex}. Estimates of the error associated with k_{rc} differ, and they range from less than 0.1 kcal/mol to a maximum value of about 0.5 kcal/mol.

perimental protection factors for the FAT domain (Figure 5) with a correlation coefficient of 0.99. In contrast, if the set of unscaled contact potentials (see the Supplemental Data for unscaled Gō model simulations) is used instead of the scaled set, the correlation coefficient is only 0.07. The set of scaled contact potentials produced from the Monte Carlo minimization of the cost function (Equation 4, see the Experimental Procedures) therefore
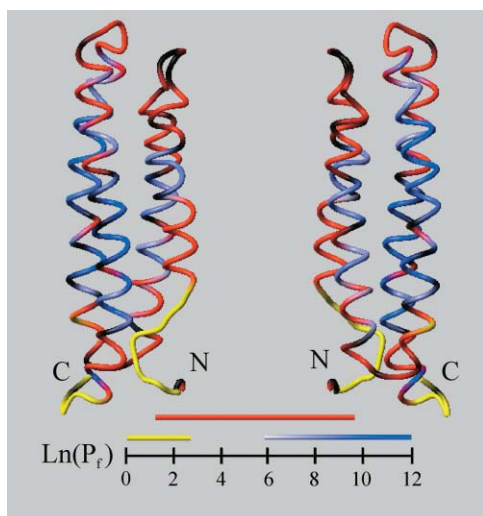
Figure 2. The FAT Domain Color-Coded by ln(P_f)

Cα trace corresponding to the lowest-energy NMR solution structure of the FAT domain, colored to reflect the natural logarithm of the protection factor. Amide protons that were observed by using the CLEANEX-PM experiments have their residues colored yellow. Amide protons with hydrogen exchange rates that were measured by using fHSQC as a function of time have their residues colored with a blue gradient displaying the protection factor on a logarithmic scale. Amide protons with hydrogen exchange rates that could not be determined by using these experiments have their residues colored red. Proline residues (which do not have amide protons) and residues containing unassigned amide protons are colored black. The scale indicates the range of protection factors spanned by each region. The figure was prepared by using MOLMOL (Koradi et al., 1996).
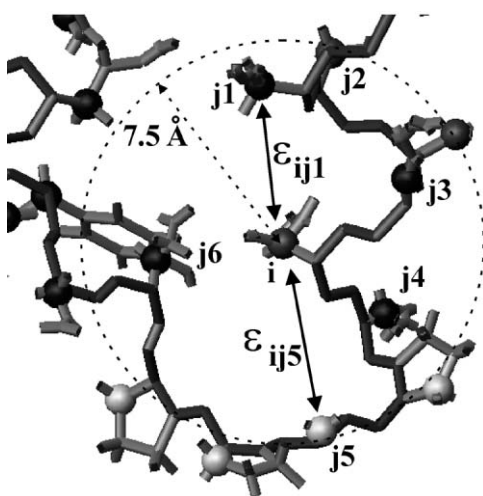

Figure 3. Native Contacts in the Folded Structure of the FAT Domain

The backbone of the protein is shown as a dark solid line, side chains are shown as lighter solid lines, and solid spheres represent the C$^\beta$ atoms (all hydrogen atoms have been omitted). Considering residue i, a native contact exists if the C$^\beta$ from any other residue (j$_1$, j$_2$, ...) is within a cutoff distance, in this case 7.5 Å. A pairwise potential, ϵ_{ij}, was assigned for each native contact. Darker spheres represent the C$^\beta$ atoms of residues for which a protection factor was measured, and lighter spheres represent C$^\beta$ atoms of residues (e.g. proline residues) for which a protection factor was not determined.
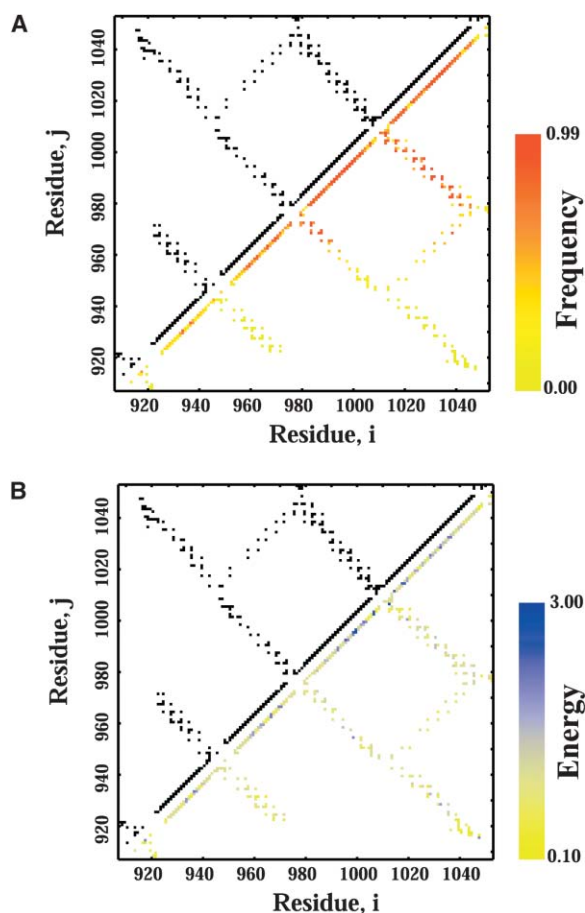

Figure 4. Contact/Energy Map for the FAT Domain and Contact/Frequency Map for the Intermediate Ensemble

(A) Contact map for the native state of the FAT domain with the pairwise contact potentials, scaled from the HX protection factors, shown in the lower right triangle. The energy scale for the contact potentials is in units of ϵ.

(B) Contact map for the FAT domain with the lower right triangle showing the frequency of the contacts in the intermediate ensemble at T = 0.72.

represents an accurate incorporation of the experimental protection factors into the DMD simulations.

To test the robustness of our method for scaling contact potentials, calculated protection factors were generated for three other proteins whose hydrogen exchange protection factors are available in the literature; barnase (Perrett et al., 1995), horse heart cytochrome C (Milne et al., 1998), and ribonuclease H (Chamberlain et al., 1996). Since the protection factors were used solely as adjustable parameters for our scaling model, it was not important how the exchange experiments were conducted or whether the EX2 limit was satisfied. Contact energies for each of these proteins were scaled according to their experimental protection factors and were then reconstituted in the form of calculated protection factors. Strong correlations were observed between the experimental and calculated protection factors (Figure 5) for all three proteins, with correlation coefficients similar to that obtained for the FAT domain. These re-
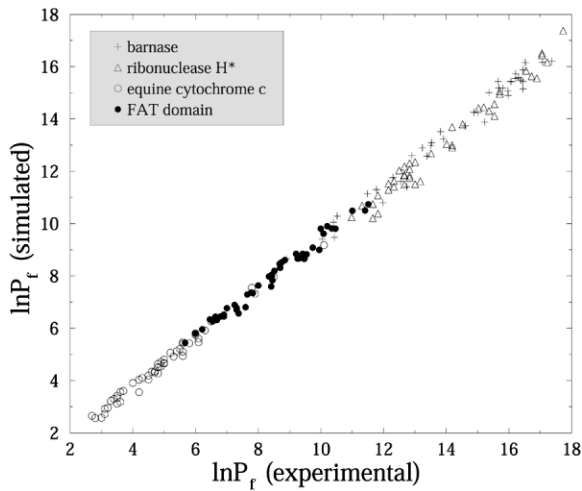
Figure 5. Correlation between Experimental and Calculated Protection Factors

Correlation plot comparing the experimentally determined protection factors with the reconstituted protection factors after the Monte Carlo scaling of the pairwise contact potentials of the FAT domain. The algorithm was applied to three other well-characterized proteins: barnase, mutant ribonuclease H, and equine cytochrome c for comparison.
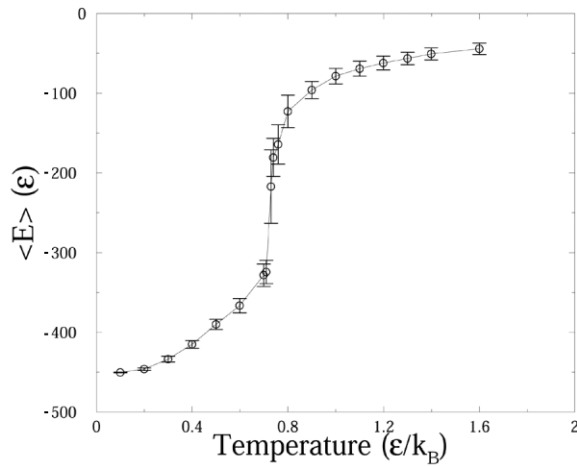

Figure 6. The Folding Trajectory for the Scaled DMD Simulations

The folding trajectory of the FAT domain from DMD simulations using the Gō model with the pairwise contacts scaled to agree with the experimentally determined protection factors. Error bars are shown depicting the standard deviation. The temperature of the simulation and the total energy of the protein are shown in reduced units based on the potential energy of the protein's native contacts, ϵ.

sults verify that our method for scaling the contact potentials is self-consistent.

Recently, Vendruscolo and coworkers (Vendruscolo et al., 2003) have proposed a phenomenological approach to utilize hydrogen exchange data to bias the sampling in conformational space toward rare fluctuations of native proteins. In contrast, our method is intended to refine the interaction model with HX data so that we can better characterize the energetics underlying the folding process. Using this method, we are able to reconstruct particular ensembles at a given temperature and also characterize the thermodynamics and kinetic parameters of the FAT domain based on the rapid DMD simulation algorithm.

The temperature dependence of the average potential energy, derived from the scaled Gō model simulation of the FAT domain, is shown in Figure 6. At low temperatures ($T \ll 1$, where the temperature is in reduced units of ϵ/k_B), the FAT domain exists predominately in its native folded state, whereas at high temperatures ($T > 1$), it is present mostly in an unfolded state. The sigmoidal curve shows a large increase of potential energy with the increase of temperature, which indicates a highly cooperative step in the transition. The shape of the curve alone does not provide the number of states that are present at a given temperature. Rather, it reflects the average potential energy over all states. To determine which states are present, we analyzed the distribution of potential energy states.

The probability distribution associated with the total potential energy of the protein is shown at three different simulation temperatures in Figure 7. At $T = 0.68$ (bottom panel), the distribution of states is concentrated in a single distribution, with an energy value near the native folded state of the protein. As the simulated temperature
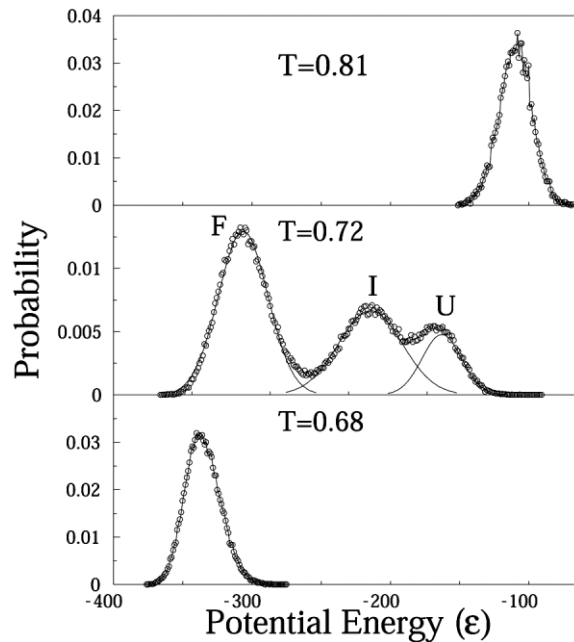

Figure 7. The Probability Distribution at Three Simulation Temperatures

The probability distribution of the total potential energy for the FAT domain, based on the summation over all pairwise contacts, for three simulated temperatures along the folding transition. At $T = 0.68$ (bottom panel), the distribution of states is concentrated in a single distribution, with an energy value near the native, folded state of the protein. As the simulated temperature is raised to 0.72 ($\sim T_M$, middle panel), three distinct distributions are apparent: a native-like folded (F) state, an intermediate (I) state, and a largely unfolded (U) state. A Gaussian fitting was used to determine the relative distribution of the three states. Near the end of the transition (top panel), $T = 0.81$, a single distribution is observed with an energy that is near the fully denatured state of the protein.

Intermediate from DMD   **FAT in Domain-swapped Dimer**
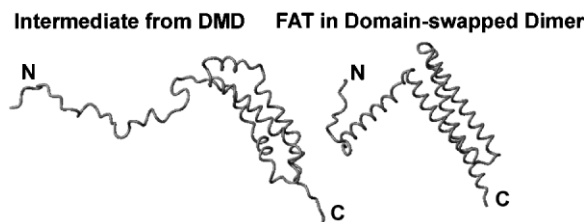

Figure 8. Comparison of the FAT Domain Intermediate from DMD Simulations with the Domain-Swapped Dimer

A single representative structure from the intermediate state ensemble is shown for comparison with a single molecule from the domain-swapped dimer crystal structure (Protein Data Bank 1K04) of the FAT domain. In both structures, helix 1 has separated from the helix bundle, and in the intermediate structure, this is accompanied by the loss of helical character in helix 1. The figure was prepared with MOLMOL (Koradi et al., 1996).

is raised to 0.72 (middle panel), three distinct distributions are apparent: a native-like folded (F) state, an intermediate (I) state, and a largely unfolded (U) state. Near the end of the transition (top panel), T = 0.81, a single distribution is observed with an energy that is near the completely unfolded state of the protein. The presence of an intermediate state is clearly detected in these distributions, and a Gaussian fitting, used to determine the relative distribution of the states, shows that the intermediate state is significantly populated near the midpoint of the transition.

The FAT Folding Intermediate

The intermediate state is not a discrete structure, but an ensemble of conformations that have potential energies that are distinct from the ensembles of the folded and unfolded states. There are two main characteristics of the intermediate detected by the scaled Gō model simulations of the FAT domain: 1) helix 1 separates from the helix bundle, and 2) helix 1 loses helical structure. The frequency map for the intermediate state at T = 0.72 is shown in the lower right triangle of Figure 4B. The frequency map indicates the probability that a contact that exists in the native state is being made at the given temperature of the simulation. Inspection of the intra-helix (along the diagonal) and interhelix (perpendicular to the diagonal) contacts indicates that contacts made by helix 1 (residues 924–943) occur with lower frequency than the contacts made by residues in the other helices.

A single FAT domain molecule from the domain-swapped dimer structure (Arold et al., 2002) is shown next to a snap shot of the folding intermediate ensemble produced by the scaled Gō simulations in Figure 8; both structures share the characteristic of having helix 1 extended from the helix bundle. The intermediate structure is weakly populated at temperatures that stabilize the four-helix bundle fold, but the population increases in the DMD simulations when the temperature of the simulation is raised sufficiently. The domain-swapped dimer structure was produced from crystals at room temperature (Arold et al., 2002), which suggests that helix 1 transiently extends from the helix bundle at temperatures well below the melting temperature (T_M = 83.4°C at pH = 6.0, unpublished data). This partitioning conse-

quently allows the domain-exchanged dimer to form. Crystals of the domain-swapped dimer only appeared after 3 months, leading the authors to speculate that helix-exchanged molecules represent a minor population of the FAT domain. Although a domain-swapped dimer form of the FAT domain has been characterized, there is little evidence to support a role for a FAK dimer in vivo (Arold et al., 2002). As such, the FAT domain-swapped dimer may be a byproduct of the FAT domain sampling a more "open" intermediate that becomes populated at concentrations used for X-ray crystallization. In contrast, mounting evidence suggests that helix 1 is conformationally dynamic, and conformational changes in helix 1 are important for phosphorylation of Y926 by Src, recognition by Grb2, initiation of MAPK signaling, subcellular localization of FAK, and focal adhesion turnover.

Discussion

The scaled Gō model simulations of the FAT domain reveal a folding intermediate ensemble in which helix 1 is less structured and separates from the helix bundle. Although the HX data indicate that residues in helix 1 are less protected than residues in helices 2–4, the HX data alone cannot confirm the presence of the intermediate state. Hydrogen exchange experiments as a function of chemical denaturant are able to detect cooperative units of unfolding (Bai et al., 1994) and subglobal unfolding and have been employed to demonstrate subglobal unfolding in the four-helix bundle protein, cytochrome b_{562} (Fuentes and Wand, 1998). We recognize that our simulations produce a subglobal opening in the FAT domain that denaturation studies may be able to experimentally confirm. However, identifying the contributions to the effective hydrogen exchange rate (i.e., local, subglobal, and global) was not necessary for our method, since scaling the native contacts was based solely on the effective exchange rate. Furthermore, using our scaled Gō model simulations, we were able to both identify cooperative units of unfolding and reconstruct coarse structures of the intermediate state.

The general features of this intermediate state are consistent with our recent solution structural studies of the FAT domain, in which line broadening associated with NH resonances in and around helix 1 and 2 led us to propose that a proline-rich "hinge region" in the FAT domain produces a strain resulting in enhanced conformational dynamics of helix 1 (Prutzman et al., 2004). Moreover, the intermediate state ensemble detected by our DMD/HX approach is consistent with the FAT domain "sampling" a more open state that leads to the formation of a domain-swapped dimer (Arold et al., 2002). The region of the FAT domain that is exposed in this intermediate state ensemble, i.e., helix 1, has been shown to play a role in FAK phosphorylation, paxillin binding, and FAK localization.

The Role of the Open and Closed Conformers of the FAT Domain

Results from this study combined with our previous observations (Prutzman et al., 2004) support the existence
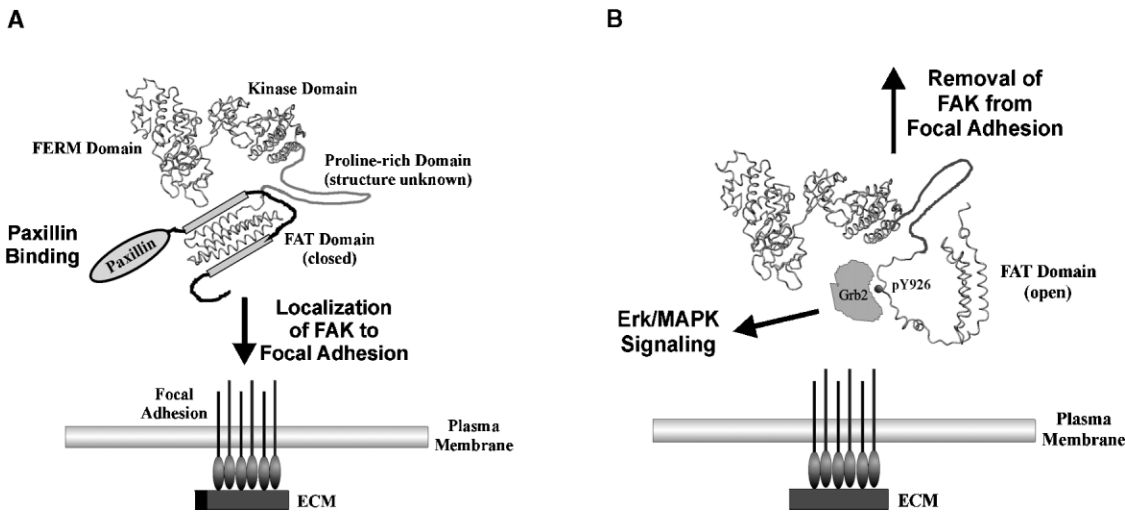
A

B

Figure 9. Working Model for the Biological Role of the Open and Closed Forms of the FAT Domain

(A and B) Contact with the extracellular matrix (ECM) stimulates integrin clustering and the formation of focal adhesions (FAs), which in turn promote recruitment of FAK to FAs. In the closed form, the FAT domain binds paxillin and localizes full-length FAK to focal adhesions. The FAT domain can also adopt an open conformation, which disrupts paxillin binding and enables Src kinases to phosphorylate Y926. Phosphorylation of Y926 creates a recognition site for Grb2, which activates Erk/MAPK signaling. Phosphorylation of Y926 also leads to the exclusion of FAK from focal adhesions, one possible mechanism for terminating FAK signaling and promoting focal adhesion turnover in migrating cells.

of "open" and "closed" conformations of the FAT domain. The four-helix bundle (closed conformation) of the FAT domain appears to be important for two distinct, yet related, processes: paxillin binding and targeting FAK to focal adhesions. Recent structural and biochemical studies have elucidated paxillin binding interactions with the FAT domain (Gao et al., 2004; Hayashi et al., 2002; Hildebrand et al., 1995; Hoellerer et al., 2003; Tachibana et al., 1995). However, the process by which FAK becomes localized to focal adhesions is not completely understood. Although the binding of paxillin and focal adhesion targeting of FAK show a strong correlation (Chen et al., 1995; Tachibana et al., 1995), studies of FAK mutants have revealed that paxillin binding is dispensable for localizing FAK to focal adhesions (Cooley et al., 2000). It has therefore been suggested that paxillin binding represents one mechanism for localizing FAK to focal adhesions and that alternative mechanism(s) exist (Cooley et al., 2000). One possible alternative mechanism involves binding of the focal adhesion protein talin (Chen et al., 1995) to the FAT domain, which may facilitate the targeting of FAK to focal adhesions. Interestingly, mutational analyses indicate that while paxillin requires an intact FAT structure for binding, talin does not (Chen et al., 1995; Hayashi et al., 2002). Therefore, the "closed form" of the FAT domain may be important for targeting FAK to focal adhesions through a paxillin binding mechanism.

Recent structures of the FAT domain complexed to paxillin-derived LD peptides indicate that paxillin binds the FAT domain at interfaces between helices 1 and 4 as well as between helices 2 and 3 (Gao et al., 2004; Hoellerer et al., 2003; Liu et al., 2002). Moreover, paxillin requires a rigid four-helix bundle conformation for FAT binding but does not induce significant structural rearrangements in the FAT domain upon binding (Gao et al., 2004; Hoellerer et al., 2003; Liu et al., 2002). The two

sites of FAT involved in paxillin LD peptide binding have been designated hydrophobic patch 1 (HP1) and 2 (HP2) (Gao et al., 2004; Hayashi et al., 2002). One of the binding sites, HP2, partially obstructs Y926 (Hayashi et al., 2002; Hoellerer et al., 2003). Not only is paxillin binding likely to interfere with phosphorylation of Y926, but mounting evidence suggests that phosphorylation and Grb2 binding to the FAT domain requires structural rearrangements within helix 1 of the FAT domain (Arold et al., 2002; Liu et al., 2002). However, structural rearrangements within helix 1 are likely to perturb the paxillin binding site at HP2, which lies between helices 1 and 4, so the conformational changes required for phosphorylation at Y926 are likely to disrupt paxillin FAT/HP2 interactions. Therefore, paxillin binding at HP2 and phosphorylation of Y926 are likely to be mutually exclusive events.

A previously reported double mutant, V955A/L962A, showed disruption of paxillin binding but retained the ability to target focal adhesions (Cooley et al., 2000). While the V955A/L962A double mutant does not cause significant structural alterations in the FAT domain (Prutzman et al., 2004), the mutations in helix 2 have been predicted to cause subtle perturbations in the four-helix bundle core of FAT by disruption of specific hydrophobic interactions between helices 2 and 3. Our labs have shown that this double mutant exhibits an approximately 8-fold increase in dimerization (by gel-filtration) and a dramatic increase in Y926 phosphorylation in vivo (Prutzman et al., 2004). The increase in dimerization suggests that the protein is more frequently sampling "open" conformations that expose hydrophobic residues within the amphipathic helices (Prutzman et al., 2004). In the same study, it was shown that helix 1, when expressed as a GST fusion protein, was phosphorylated approximately 8-fold more than a GST-FAT domain fusion protein (Prutzman et al., 2004). We have

previously postulated that the increased phosphorylation, dimerization, and disruption of paxillin binding observed for the V955A/L962A FAT variant may be the result of conformational dynamics involving helix 1 (Prutzman et al., 2004).

We have proposed a model for the role of FAT conformational dynamics in FAK-mediated cell adhesion and signaling processes, based on the available structural, biochemical, and biological information on FAK combined with structures produced from the scaled Gō model simulations. In our model, the open conformation of the FAT domain is important for FAK signaling. Phosphorylation of Y926 creates a consensus recognition site (pYNQV) for the SH2 domain of Grb2 (Rahuel et al., 1996). However, phosphorylation and subsequent binding requires a more extended conformation of helix 1 (Rahuel et al., 1996), and therefore helix 1 must have some degree of conformational flexibility to accommodate the required structural rearrangements (Arold et al., 2002; Liu et al., 2002). Grb2 binding at pY926 initiates signaling through the Ras/MAPK pathway. Therefore, transient population of the intermediate state conformers could favor the structural rearrangements of helix 1 that facilitate Grb2 activation of the MAPK pathway.

We also postulate that the open conformation aids in the removal of FAK from focal adhesions, as phosphorylation of Y926 has been linked to exclusion of FAK from focal adhesions (Katz et al., 2003). Moreover, based on current structural data, it has been speculated that the SH2 domain of Grb2 cannot bind phosphorylated Y926 while FAK is still associated with the focal adhesion complex (Liu et al., 2002). Although the precise sequence of events is not known, we speculate that the open conformer of FAT, once phosphorylated, initiates FAK-mediated MAPK signaling and also promotes the removal of FAK from focal adhesions.

Working Model of the FAT Domain

A summary of our working model is shown in Figure 9. Data obtained from this study, as well as our previous study (Prutzman et al., 2004), provide tangible evidence for a biologically significant open conformation of the FAT domain. Our working model emphasizes the importance of conformational dynamics in the FAT domain on the subcellular localization of FAK, ligand binding interactions, and integrin-mediated FAK signaling. We are in the process of characterizing FAT mutants that possess altered helix 1 dynamics to test this working model.

Experimental Procedures

Expression and Purification of the FAT Domain of FAK
The FAT domain, containing residues 920–1053 of avian FAK plus a 12 amino acid N-terminal linker, was expressed as a GST fusion protein (Thomas et al., 1999) and was purified as previously described (Gao et al., 2004).

NMR Sample Preparation
Purified proteins were exchanged into NMR buffer (25 mM Tris-d$_{11}$ Maleate-d$_2$ [pH 6.0], 150 mM NaCl, 0.1% NaN$_3$, PPACK [1 μM], pefabloc [0.5 mg/ml] and 10% D$_2$O) by using an Amicon Ultra centrifugal filter device (MW cutoff 10,000). The FAT domain was then concentrated to 0.5 mM and transferred to a Wilmad NMR tube.

The final concentration of the protein was determined by using the BCA protein assay (Pierce Biotechnology, Inc.).

To rapidly change the NMR buffer to a D$_2$O-based buffer, the NMR sample containing the purified protein was concentrated to 0.25 ml by centrifugation in an Amicon Ultra centrifugal filter device, then eluted on a PD-10 gel filtration column (Amersham Biosciences) that was equilibrated with 25 ml deuterated NMR buffer (25 mM Tris-d$_{11}$ Maleate-d$_2$ [pH$_{read}$ 5.6], 150 mM NaCl, 0.1% NaN$_3$, PPACK [1 μM], pefabloc [0.5 mg/ml], and D$_2$O [99.9%, Cambridge Isotope Laboratories]). Elution fractions were collected in 0.5 ml portions and analyzed for protein by using a BioRad protein assay. Fractions containing protein were combined and transferred to a Wilmad NMR tube. Data collection typically began 25 min after the protein was loaded on the PD-10 column.

NMR Data Collection and Analysis
Fast 2D ^{1}H-^{15}N heteronuclear single quantum coherence (fHSQC) data were collected on a Varian INOVA 800-MHz spectrometer at 37°C to monitor the loss of the protein backbone amide ^{1}H signal as a function of time. Each fHSQC data set was acquired in 10 min and 30 s, with the halfway point of the experiment used as the time point for data analysis. A total of 1024 (^{1}H) × 256 (^{15}N) complex points were collected over spectral windows of 16.7 ppm (^{1}H) and 29.6 ppm (^{15}N). NMR spectra were processed with NMRPipe (Delaglio et al., 1995) and analyzed with NMRView (Johnson and Blevins, 1994). Hydrogen exchange rates were determined from the slopes of best-fit lines, by fitting the logarithm of the peak intensities versus time, by using SigmaPlot 2001 on a Windows XP platform using the method of initial rates.

CLEANEX-PM experiments (Hwang et al., 1997; Hwang et al., 1998) were performed on a Varian INOVA 600-MHz spectrometer at 37°C. A Gaussian-shaped pulse (7.5 ms) was employed to selectively saturate the water resonance, and mixing times of 5, 10, 15, 20, and 25 ms were used. A total of 1024 (^{1}H) × 128 (^{15}N) complex points were collected over spectral windows of 16.3 ppm (^{1}H) and 22.2 ppm (^{15}N). NMR spectra were processed with NMRPipe (Delaglio et al., 1995) and analyzed with NMRView (Johnson and Blevins, 1994).

Discrete Molecular Dynamics Simulations
Interaction Model
A discrete molecular dynamics (DMD) algorithm (Dokholyan et al., 1998; Smith et al., 1997; Zhou et al., 1997) was used to study the folding thermodynamics of the FAT domain, as DMD simulations have proven to be very useful in the study of folding kinetics (Borreguero et al., 2002; Ding et al., 2002a; Zhou and Karplus, 1999a; Zhou and Karplus, 1999b) and aggregation of proteins (Ding et al., 2002b; Smith and Hall, 2001). The FAT domain was modeled by using the "beads-on-string" method developed by Ding et al. (Ding et al., 2003), with "beads" corresponding to the C$^\alpha$, C$^\beta$, N, and C' atoms. During the simulation, distance and angle constraints are maintained between the "bead" atoms. The lowest energy solution structure, determined by NMR (Prutzman et al., 2004), was used as the native structure, and the Gō potential was employed to model the interaction energy between native contacts. The nonbonded interactions, V_{ij}, were only assigned between C$^\beta$ atoms (C$^\alpha$ for Gly) of residues i and j ($|i - j| > 2$):

$$V_{ij} = \begin{cases} +\infty, & |r_i - r_j| \le a \\ \gamma\epsilon_{ij}, & a < |r_i - r_j| < b \\ 0, & |r_i - r_j| > b, \end{cases} \quad (2)$$

where $|r_i - r_j|$ is the distance between C$^\beta$ atoms (C$^\alpha$ for Gly) of residues i and j. The parameters a and b are the hard-core diameter (3.25 Å) and the cutoff distance (7.5 Å), respectively. If the C$^\beta$ atoms (C$^\alpha$ for Gly) for a pair of residues are closer than 7.5 Å in the native state, an attractive potential ($\gamma = -1$) was assigned to the pairwise interaction; a repulsive potential ($\gamma = 1$) was assigned for the interaction between all pairs of residues whose C$^\beta$ atoms (C$^\alpha$ for Gly) were separated by more than 7.5 Å in the native state. The depths of the attractive square-well, ϵ_{ij} in Equation 2, are equal in the *unscaled* Gō model, whereas in the *scaled* Gō model, ϵ_{ij} is assigned different strengths according to experimental data, as described below.

Scaling Gō Model Potentials with Experimental Protection Factors

Since the measurements of the protection factors were performed under conditions in which the folded state is dominant, we expect that hydrogen exchange for most of the residues is governed by the local fluctuation around the native structure. In the EX2 limit, where the protection factors can be used to determine the free energy associated with local protein stability, the measured protection factors can be related to the Gō model interaction energy according to Equation 3 (see the details in the Supplemental Data):

$$\ln P_i \approx \sum_j f_{ij}^F \, \epsilon_{ij} \approx \sum_j \epsilon_{ij}, \qquad (3)$$

where the summation is taken over all residues j forming native contacts with the residue i, and f_{ij}^F represents the probability of contact formation between residues i and j in the native state ensemble. We expect that the values of f_{ij}^F are approximately 1. Thus, in Equation 3, the protection factor reflects the heterogeneity in the contact energies.

The experimental protection factors were quantitatively determined for the subset of residues that could be monitored in real time. While some of the remaining residues could be approximated based on the CLEANEX-PM experiments, we did not calculate protection factors for residues that were not assigned in the ^{1}H-^{15}N HSQC NMR spectrum or for which we could not determine the observed hydrogen exchange rate by using the experiments performed. So, to determine the set $\{\epsilon_{ij}\}$ that is most consistent with the experimental data, a cost function was constructed that was minimized by using a Monte Carlo algorithm:

$$W = \left\langle \left(\ln P_{f_i} - \sum_j \epsilon_{ij} \right)^2 \right\rangle_{measured} + \left\langle \left(\epsilon_{ij} - <\epsilon_{ij}>_{all} \right)^2 \right\rangle_{all}, \; \epsilon_{ij} \geq 0.1. \qquad (4)$$

In the first term, the summation of j is taken over residues forming native contacts with i. $<...>_{measured}$ is the average taken over all the residues i with measured protection factors. For residues that were observed by using the CLEANEX-PM experiment, a small protection factor was assigned with a value of 10, as the results are not sensitive to the exact magnitude of this value. In the second term, $<...>_{all}$ is the average taken over all of the native contacts. The purpose of including the second term was to determine the pairwise contact energies for residues that were not directly constrained by available experimental data, such as contacts between residues in which neither member of the pair has a measured or approximated protection factor. All native contact energies were constrained to have a minimum attraction interaction of 0.1.

Supplemental Data

Supplemental Data including the results of unscaled Gō model simulations on the FAT domain, a more thorough derivation of the method used to scale the native contact potentials in the scaled Gō model simulations, details of the chemical denaturation studies on the FAT domain, and the complete set of the NMR hydrogen exchange data are available at http://www.structure.org/cgi/content/full/12/12/2161/DC1/.

References

Abe, H., and Gō, N. (1981). Noninteracting local structure model of folding and unfolding transition in globular proteins. II. Formulation. Biopolymers 20, 1013–1031.

Arold, S.T., Hoellerer, M.K., and Noble, M.E.M. (2002). The structural basis of localization and signaling by the focal adhesion targeting domain. Structure 10, 319–327.

Bai, Y., Milne, J.S., Mayne, L., and Englander, S.W. (1993). Primary structure effects on peptide group hydrogen exchange. Proteins 17, 75–86.

Bai, Y., Milne, J.S., Mayne, L., and Englander, S.W. (1994). Protein stability parameters measured by hydrogen exchange. Proteins 20, 4–14.

Bai, Y., Sosnick, T.R., Mayne, L., and Englander, S.W. (1995). Protein folding intermediates: native-state hydrogen exchange. Science 269, 192–197.

Borreguero, J.M., Dokholyan, N.V., Buldyrev, S.V., Stanley, H.E., and Shakhnovich, E.I. (2002). Thermodynamics and folding kinetics analysis of the SH3 domain from discrete molecular dynamics. J. Mol. Biol. 318, 863–876.

Brown, N.R., Noble, M.E.M., Endicott, J.A., and Johnson, L.N. (1999). The structural basis for specificity of substrate and recruitment peptides for cyclin-dependent kinases. Nat. Cell Biol. 1, 438–443.

Chamberlain, A.K., Handel, T.M., and Marqusee, S. (1996). Detection of rare partially folded molecules in equilibrium with the native conformation of RNaseH. Nat. Struct. Biol. 3, 782–787.

Chen, H.-C., Appeddu, P.A., Parsons, J.T., Hildebrand, J.D., Schaller, M.D., and Guan, J.-L. (1995). Interaction of focal adhesion kinase with cytoskeletal protein talin. J. Biol. Chem. 270, 16995.

Clementi, C., Garcia, A., and Onuchic, J.N. (2003). Interplay among tertiary contacts, secondary structure information and side-chain packing in the protein folding mechanism: an all-atom representation study. J. Mol. Biol. 326, 933–954.

Cooley, M.A., Broome, J.M., Ohngemach, C., Romer, L.H., and Schaller, M.D. (2000). Paxillin binding is not the sole determinant of focal adhesion localization or dominant-negative activity of focal adhesion kinase/focal adhesion kinase-related nonkinase. Mol. Biol. Cell 11, 3247–3263.

Delaglio, F., Grzesiek, S., Vuister, G.W., Zhu, G., Pfeifer, J., and Bax, A. (1995). NMRPipe: a multidimensional spectral processing system based on UNIX pipes. J. Biomol. NMR 6, 277–293.

Ding, F., Borreguero, J.M., Buldyrev, S.V., Stanley, H.E., and Dokholyan, N.V. (2003). A mechanism for the alpha-helix to beta-hairpin transition. Proteins 53, 220–228.

Ding, F., Dokholyan, N.V., Buldyrev, S.V., Stanley, H.E., and Shakhnovich, E.I. (2002a). Direct molecular dynamics observation of protein folding transition state ensemble. Biophys. J. 83, 3525–3532.

Ding, F., Dokholyan, N.V., Buldyrev, S.V., Stanley, H.E., and Shakhnovich, E.I. (2002b). Molecular dynamics simulation of C-Src SH3 aggregation suggests a generic amyloidogenesis mechanism. J. Mol. Biol. 324, 851–857.

Dokholyan, N.V., Buldyrev, S.V., Stanley, H.E., and Shakhnovich, E.I. (1998). Molecular dynamics studies of folding of a protein-like model. Fold. Des. 3, 577–587.

Fuentes, E.J., and Wand, A.J. (1998). Local dynamics and stability of apocytochrome b562 examined by hydrogen exchange. Biochemistry 37, 3687–3698.

Gabarra-Niecko, V., Schaller, M.D., and Dunty, J.M. (2003). FAK regulates biological processes important for the pathogenesis of cancer. Cancer Metastasis Rev. 22, 359–374.

Gao, G., Prutzman, K.C., King, M.L., Scheswohl, D.M., DeRose, E.F., London, R.E., Schaller, M.D., and Campbell, S.L. (2004). NMR solution structure of the focal adhesion targeting domain of focal adhesion kinase in complex with a Paxillin LD peptide: evidence for a two site binding model. J. Biol. Chem. 279, 8441–8451.

Gō, N., and Abe, H. (1981). Noninteracting local structure model of folding and unfolding transition in globular proteins. I. Formulation. Biopolymers 20, 991–1011.

Hayashi, I., Vuori, K., and Liddington, R.C. (2002). The focal adhesion targeting (FAT) region of focal adhesion kinase is a four-helix bundle that binds paxillin. Nat. Struct. Biol. *9*, 101–106.

Hildebrand, J., Schaller, M., and Parsons, J. (1995). Paxillin, a tyrosine phosphorylated focal adhesion-associated protein binds to the carboxyl terminal domain of focal adhesion kinase. Mol. Biol. Cell *6*, 637–647.

Hildebrand, J.D., Schaller, M.D., and Parsons, J.T. (1993). Identification of sequences required for the efficient localization of the focal adhesion kinase, pp125FAK, to cellular focal adhesions. J. Cell Biol. *123*, 993.

Hoellerer, M.K., Noble, M.E.M., Labesse, G., Campbell, I.D., Werner, J.M., and Arold, S.T. (2003). Molecular recognition of paxillin LD motifs by the focal adhesion targeting domain. Structure *11*, 1207–1217.

Hubbard, S.R. (1997). Crystal structure of the activated insulin receptor tyrosine kinase in complex with peptide substrate and ATP analog. EMBO J. *16*, 5572–5581.

Hwang, T.-L., Mori, S., and van Zijl, P.C.M. (1997). Application of Phase-Modulated CLEAN chemical EXchange spectroscopy (CLEANEX-PM) to detect water-protein proton exchange and intermolecular NOEs. J. Am. Chem. Soc. *119*, 6203–6204.

Hwang, T.-L., van Zijl, P.C.M., and Mori, S. (1998). Accurate quantitation of water-amide proton exchange rates using the Phase-Modulated CLEAN chemical EXchange (CLEANEX-PM) approach with a Fast-HSQC (FHSQC) detection scheme. J. Biomol. NMR *11*, 221–226.

Johnson, B., and Blevins, R.A. (1994). NMRView: a computer program for the visualization and analysis of NMR data. J. Biomol. NMR *4*, 603–614.

Karanicolas, J., and Brooks, C.L., III. (2002). The origins of asymmetry in the folding transition states of protein L and protein G. Protein Sci. *11*, 2351–2361.

Karplus, M., and Shakhnovich, E.I. (1994). Protein folding: theoretical studies of thermodynamics and dynamics. In Protein Folding, T. Creighton, ed. (New York, W.H. Freeman & Company), pp. 127–196.

Katz, B.-Z., Romer, L., Miyamoto, S., Volberg, T., Matsumoto, K., Cukierman, E., Gieger, B., and Yamada, K.M. (2003). Targeting membrane-localized FAK to focal adhesions: roles of tyrosine phosphorylation and Src family kinases. J. Biol. Chem. *278*, 29115–29120.

Khare, S.D., Ding, F., and Dokholyan, N.V. (2003). Folding of Cu, Zn superoxide dismutase and familial amyotrophic lateral sclerosis. J. Mol. Biol. *334*, 515–525.

Kuriyan, J., and Cowburn, D. (1997). Modular peptide recognition domains in eukaryotic signaling. Annu. Rev. Biophys. Biomol. Struct. *26*, 259–288.

Liu, G., Guibao, C.D., and Zheng, J. (2002). Structural insight into the mechanisms of targeting and signaling of focal adhesion kinase. Mol. Cell. Biol. *22*, 2751–2760.

Maity, H., Lim, W.K., Rumbley, J.N., and Englander, S.W. (2003). Protein hydrogen exchange mechanism: local fluctuations. Protein Sci. *12*, 153–160.

Mayne, L., and Englander, S.W. (2000). Two-state vs. multistate protein unfolding studied by optical melting and hydrogen exchange. Protein Sci. *9*, 1873–1877.

Milne, J.S., Mayne, L., Roder, H., Wand, A.J., and Englander, S.W. (1998). Determinants of protein hydrogen exchange studied in equine cytochrome c. Protein Sci. *7*, 739–745.

Parsons, J.T. (2003). Focal adhesion kinase: the first ten years. J. Cell Sci. *116*, 1409–1416.

Perrett, S., Clarke, J., Hounslow, A.M., and Fersht, A.R. (1995). Relationship between equilibrium amide proton exchange behavior and the folding pathway of barnase. Biochemistry *34*, 9288–9298.

Prutzman, K.C., Gao, G., King, M.L., Iyer, V.V., Mueller, G.A., Schaller, M.D., and Campbell, S.L. (2004). The focal adhesion targeting domain of focal adhesion kinase contains a hinge region that modulates tyrosine 926 phosphorylation. Structure *12*, 881–891.

Rahuel, J., Gay, B., Erdmann, D., Strauss, A., Garcia-Echeverria, C.,

Furet, P., Caravatti, G., Fretz, H., Schoepfer, J., and Grutter, M. (1996). Structural basis for specificity of Grb2–SH2 revealed by a novel ligand binding mode. Nat. Struct. Biol. *3*, 586–589.

Santoro, M.M., and Bolen, D.W. (1988). Unfolding free energy changes determined by the linear extrapolation method. 1. Unfolding of phenylmethanesulfonyl a-chymotrypsin using different denaturants. Biochemistry *27*, 8063–8068.

Schaller, M.D. (2001). Biochemical signals and biological responses elicited by the focal adhesion kinase. Biochim. Biophys. Acta *1540*, 1–21.

Schlaepfer, D.D., and Hunter, T. (1996). Evidence for in vivo phosphorylation of the Grb2 SH2-domain binding site on focal adhesion kinase by Src-family protein-tyrosine kinases. Mol. Cell. Biol. *16*, 5623–5633.

Schlaepfer, D.D., and Hunter, T. (1997). Focal adhesion kinase overexpression enhances ras-dependent integrin signaling to ERK2/mitogen-activated protein kinase through interactions with and activation of c-Src. J. Biol. Chem. *272*, 13189–13195.

Shen, Y., and Schaller, M.D. (1999). Focal adhesion targeting: the critical determinant of FAK regulation and substrate phosphorylation. Mol. Biol. Cell *10*, 2507–2518.

Smith, A.V., and Hall, C.K. (2001). Protein refolding versus protein aggregation: computer simulations on an intermediate-resolution protein model. J. Mol. Biol. *312*, 187–202.

Smith, S.W., Hall, C.K., and Freeman, B.D. (1997). Molecular dynamics for polymeric fluids using discontinuous potentials. J. Comput. Phys. *134*, 917–951.

Tachibana, K., Sato, T., D'Avirro, N., and Morimoto, C. (1995). Direct association of pp125FAK with paxillin, the focal adhesion-targeting mechanism of pp125FAK. J. Exp. Med. *182*, 1089–1099.

Thomas, J.W., Cooley, M.A., Broome, J.M., Salgia, R., Griffin, J.D., Lombardo, C.R., and Schaller, M.D. (1999). The role of focal adhesion kinase binding in the regulation of tyrosine phosphorylation of paxillin. J. Biol. Chem. *274*, 36684–36692.

Vendruscolo, M., Paci, E., Dobson, C.M., and Karplus, M. (2003). Rare fluctuations of native proteins sampled by equilibrium hydrogen exchange. J. Am. Chem. Soc. *125*, 15686–15687.

Zhou, Y., and Karplus, M. (1999a). Folding of a model three-helix bundle protein: a thermodynamic and kinetic analysis. J. Mol. Biol. *293*, 917–951.

Zhou, Y., and Karplus, M. (1999b). Interpreting the folding kinetics of helical proteins. Nature *401*, 400–403.

Zhou, Y., Karplus, M., Wichert, J.M., and Hall, C.K. (1997). Equilibrium thermodynamics of homopolymers and clusters: molecular dynamics and Monte Carlo simulations of system with square-well interactions. J. Chem. Phys. *107*, 10691–10708.